Geomechanics and Engineering, *Vol. 24, No. 1 (2021) 81-89*
DOI: https://doi.org/10.12989/gae.2021.24.1.081

Effects of interface angles on properties of rock-cemented coal gangue-fly ash backfill bi-materials

Da W. Yin[1,2a], Shao J. Chen*[1], Xi Z. Sun[3b] and Ning Jiang[1c]

[1]*State Key Laboratory of Mine Disaster Prevention and Control, Shandong University of Science and Technology, Qingdao 266590, China*
[2]*Key Laboratory of Safety and High-efficiency Coal Mining, Ministry of Education, Anhui University of Science and Technology, Huainan 232001, China*
[3]*College of Civil Engineering and Architecture, Linyi University, Linyi 276000, China*

(Received August 25, 2020, Revised December 22, 2020, Accepted December 28, 2020)

Abstract. Uniaxial compression tests were conducted on sandstone-CGFB composite samples with different interface angles, and their strength, acoustic emission (AE), and failure characteristics were investigated. Three macro-failure patterns were identified: the splitting failure accompanied by local spalling failure in CGFB (Type-I), the mixed failure with small sliding failure along with the interface and Type-I failure (Type-II), and the sliding failure along with the interface (Type-III). With an increase of interface angle β measured horizontally, the macro-failure pattern changed from Type-I to Type-II, and then to Type-III, and the uniaxial compressive strength and elastic modulus generally decreased. Due to the small sliding failure along with the interface in the composite sample with β of 45°, AE events underwent fluctuations in peak values at the later post-peak failure stage. The composite samples with β of 60° occurred Type-III failure before the completion of initial compaction stage, and the post-peak stress-time curve initially exhibited a slow decrease, followed by a steep linear drop with peaks in AE events.

Keywords: rock-cemented coal gangue-fly ash backfill bi-materials; interface angle; strength characteristics; failure mechanism; uniaxial loading

1. Introduction

The exploitation of coal resources can induce the surface subsidence and ecological environment destruction (Ammirati *et al.* 2020, Tichavsky *et al.* 2020, Ozdogan *et al.* 2020, Scigala and Szafulera 2020, Strzalkowski and Szafulera 2020). Backfill mining is generally used in coal mines to control the surface subsidence and to protect the ecological environment (Sivakugan *et al.* 2006, Park *et al.* 2014, Ercikdi *et al.* 2009, Cao *et al.* 2019, Tan *et al.* 2019, Wang *et al.* 2020, Bull and Fall 2020). The paste backfill materials called cemented coal gangue-fly ash backfill (CGFB), are often used in coal mines due to their high integrity and stability (Sun *et al.* 2019, Zhang *et al.* 2017). CGFB is a kind of cement composites, mainly consisting of cement, fly ash (industrial wastes from the coal-consumed power plant), coal gangue (solid wastes from coal production and coal washing process), and water. The properties of backfill materials are the kernel of backfill mining effects (Kaliyavaradhan *et al.* 2019, Mbonimpa *et al.* 2019, Zhang *et al.* 2017, Wang *et al.* 2020). Therefore, an investigation of the properties of CGFB is necessary.

Experiments are effective methods for studying the properties of CGFB samples, and research results can identify the deformation and failure evolution laws for CGFB. Many experimental investigations regarding the properties of CGFB samples have been conducted. Qi *et al.* (2015) and Ren *et al.* (2014) studied the effects of the fly ash content on the properties of CGFB samples. They found that with an increase of the fly ash content, the rheological property of CGFB sample abated; the adhesiveness was enhanced, and the bleeding index and dry shrinkage decreased. The corresponding strength was directly proportional to the fly ash content. Wang *et al.* (2018) found that the slump, divergence, setting time and compressive strength of CGFB samples increased and then decreased with the fine coal gangue content. Zhang and Wang found (2007) that the quality indices such as strength and dewatering ratios, and the piping feature of a slurry could satisfy the requirements for the cement backfill if the mass ratio of cement to fly ash to gangue was 1 : 4 : 15, and the mass fraction of solid material ranged from 72% to 75%. Chen *et al.* (2016) found that the creep strength of CGFB sample was larger than its uniaxial compressive strength (UCS), and this phenomenon was labelled the creep macro-hardening effect. Through the uniaxial compression tests on CGFB column samples (length × width × height = 800 mm × 800 mm × 1600 mm) with stirrups, Du *et al.* (2019) found that the stirrups can prevent the sudden instability of a CGFB column under uniaxial loading. Feng *et al.* (2019) studied the resistivity, AE, and ultrasonic characteristics in

*Corresponding author, Professor
E-mail: csjwyb@163.com
[a]Ph.D.
E-mail: 949251142@qq.com
[b]Ph.D.
E-mail: 496661950@qq.com
[c]Ph.D.
E-mail: jiangning198961@163.com

ISSN: 2005-307X (Print), 2092-6219 (Online)

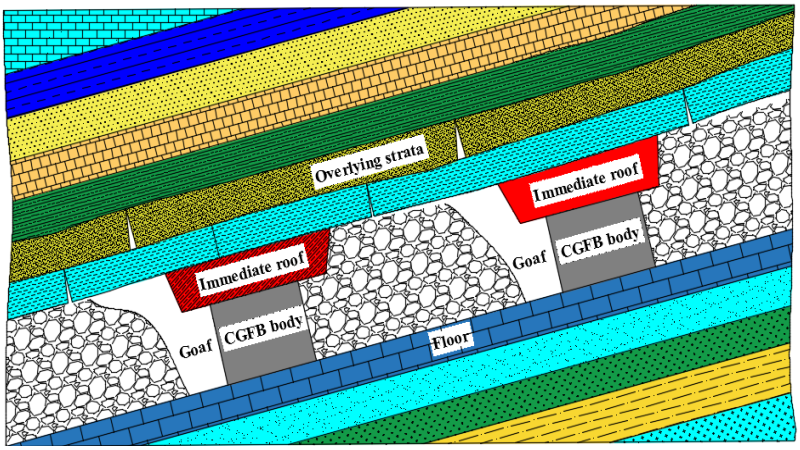

Fig. 1 Basic principles of inclined strip CGFB mining

the failure process of CGFB samples under uniaxial loading. They found that the AE ringing count signal response was more sensitive to the pore compression and micro-crack generation in initial compaction stage and elastic compression stage, and the DIC (Digital Image Correlation) response and UT (Ultrasonic Testing) response could be used to quantitatively evaluate the damage degree of the specimen. Liu *et al.* (2018) and Cui *et al.* (2018) investigated the effects of different sulphate levels on the mechanical properties of CGFB samples under uniaxial loading. They found that the uniaxial compressive strength first increased and then decreased with the soaking time and concentration in sulfate solution. Wu *et al.* (2018) developed a THMC (thermal, hydraulic, mechanical and chemical) model to analyze the temperature, pore water pressure, water drainage, lateral pressure, as well as stress-strain development of hydrating CGFB. Sun *et al.* (2019) invented a type of paste backfill material called geopolymer cemented coal gangue-fly ash backfill (GCGFB), which consisted of coal gangue, fly ash, cement, slag, and alkaline activator mixed with sodium hydroxide and sodium silicate.

The aforementioned investigations are important for understanding the properties of CGFB. Because of the continuous reductions in available backfill materials and high filling costs, the strip CGFB mining has been used to control the surface subsidence in many Chinese coal mines (Zhu *et al.* 2017, Xu *et al.* 2015, Zhu *et al.* 2019). The basic principles of this method depend on the requirements of the surface subsidence being controlled. Some strip CGFB bodies with regular intervals are arranged in the goaf to support the overlying strata and to control the surface subsidence. If the intervals between the CGFB bodies break the caving step distance of the immediate roof, the immediate roof will collapse and the broken rocks backfill the goaf, as shown in Fig. 1. Here, the composite structures of the immediate roof and CGFB body are formed in the goaf, thus supporting the overlying strata and controlling the surface subsidence. In other words, the properties of this composite structure determine the effects of controlling surface subsidence using the strip CGFB mining method. Under the inclined strip CGFB mining, the interface angle between the immediate roof and CGFB body affects the properties of the composite structure.

Many studies have been conducted to investigate the properties of rock-concrete (RC) bi-materials through the laboratory tests on the RC composite samples (a diameter of 50 mm and a height of 100 mm), including their shear failure characteristics (Fishman 2008, Sujatha and Kishen 2003), failure mechanisms (Fishman 2009, Zhong *et al.* 2014), and tensile performances (Chang *et al.* 2018). Wang *et al.* (2020) studied the effects of coal gangue particle sizes on the properties of sandstone-cemented coal gangue-fly ash backfill bimaterials. However, few studies have focused on the properties of rock-CGFB bi-materials. In this study, the sandstone-CGFB composite samples with different interface angles ranging from 0 to 60° measured horizontally, were prepared, and uniaxial compression tests were conducted on them. The effects of interface angle on the strength, AE, and failure characteristics of the composite samples were studied. This investigation could offer insights into the properties of the rock-CGFB bi-materials, which are important in ensuring the stability of the composite structure of the immediate roof and CGFB body in the inclined strip CGFB mining.

2. Material and methods

2.1 Material properties

The rock-CGFB bi-materials consisted of two different parts: rock and CGFB. The rock material used for this investigation was sandstone collected from the Daizhuang coal mine of Shandong Province, China. CGFB included the coal gangue collected from the Daizhuang coal mine, secondary fly ash obtained from the Shandong Huangdao Power Plant, Portland cement Grade 42.5 obtained from Shandong Rizhao No.3 Cement Plant, and tap water. Their chemical components are shown in Table 1. The solid materials of CGFB in the composite samples comprised 78% of the total weight of the CGFB, the mass ratio of cement to fly ash to gangue was 1 : 4 : 6, and the particle size of the coal gangue ranged from 0.1 mm to 12 mm.

According to the standard testing method of International Society for Rock Mechanics (ISRM), the uniaxial compression tests were conducted on the pure

Table 1 Chemical components of the cement, fly ash and coal gangue (unit: %)

Major element	Cement	Fly ash	Coal gangue
Na_2O	2.177	1.456	1.758
MgO	8.706	3.914	3.088
Al_2O_3	12.34	39.724	30.177
SiO_2	15.722	37.855	39.987
SO_3	3.025	1.221	2.886
K_2O	1.203	2.118	2.643
CaO	51.643	6.214	11.727
TiO_2	1.031	2.479	2.531
MnO_2	0.19	0.055	—
Fe_2O_3	3.891	4.856	4.928
ZnO	0.072	0.107	—
BaO	—	—	0.276

Table 2 Mechanical properties of pure sandstone and CGFB samples under uniaxial loading

Material	UCS/MPa	Elastic modulus/GPa (the slope of the stress-strain curve at 40-60% of peak stress)	Peak strain/%
Pure sandstone sample	40.178	5.73	1.032
Pure CGFB sample	3.538	1.07	0.492

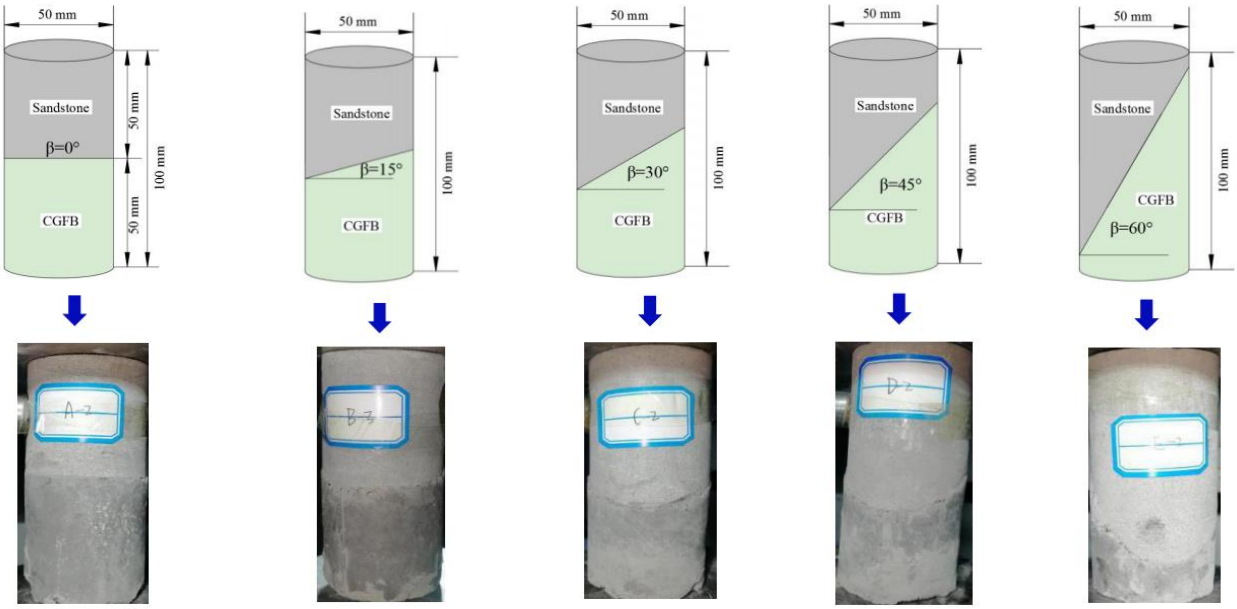

(a) β of 0° (b) β of 15° (c) β of 30° (d) β of 45° (e) β of 60°

Fig. 2 Sandstone-CGFB composite samples with different interface angles of β with respect to the horizontal direction

samples (a diameter of 50 mm and a height of 100 mm) of sandstone and CGFB (curing for 28 d with a temperature of 20 ± 2°C and a humidity of 80%) to obtain their mechanical properties, and the test results are shown in Table 2.

2.2 Sample preparation

Based on the standard testing method of ISRM and previous investigations on the properties of RC composite samples (Fishman 2008, Sujatha and Kishen 2003, Fishman 2009, Zhong *et al.* 2014, Chang *et al.* 2018, Chen *et al.* 2019a), the diameter and height of sandstone-CGFB composite samples were 50 mm and 100 mm, respectively, which are shown in Fig. 2. The interface incline angle β measured horizontally between the sandstone and CGFB ranged from 0° to 60°. A total of 15 composite samples were prepared and categorized under Groups A, B, C, D, and E, corresponding to β of 0°, 15°, 30°, 45°, and 60°, respectively. Each group had three composite samples.

During the composite sample preparation, the sandstone blocks were first processed into the cylindrical samples with

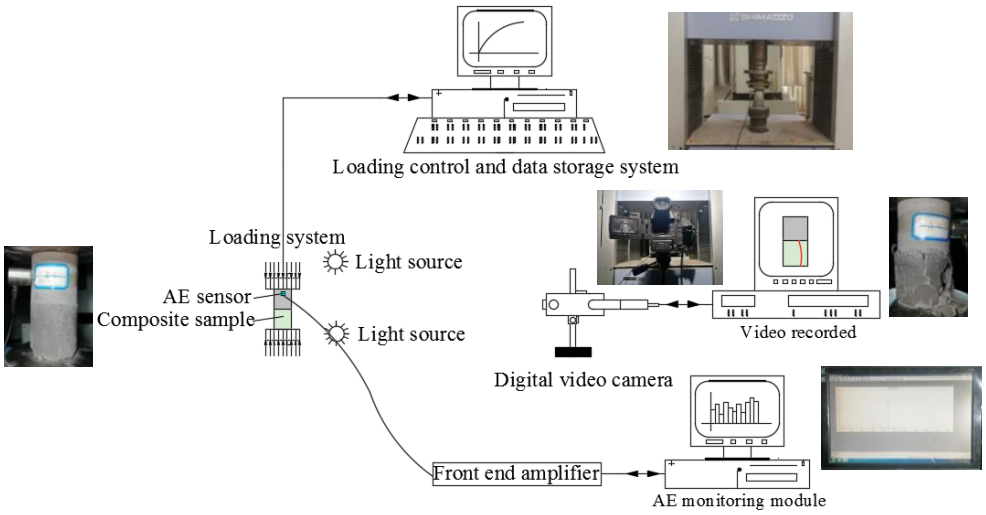

Fig. 3 Testing system for uniaxial compression tests with composite samples

Table 3 AE parameters

Main amplifier	40 dB	AE probe type	R3α
Threshold value	45 dB	Resonant frequency of AE probe type	~20-100 kHz
Floating threshold	6 dB	Sampling frequency	10^6/s

a diameter of 50 mm and a height of 100 mm. The cylindrical sandstone samples were cut into two equal parts and interface angles ranging from 0° to 60° measured horizontally using a stone-sawing machine. Then both ends of the samples were flattened, and smoothed using a stone-grinding machine in order to meet the test requirements. Each sandstone piece was then placed in the mould with a diameter of 51 mm and a height of 100 mm, with its cutting surface at the top. Then the well stirred mixtures of CGFB were directly poured into the moulds, thus filling the remaining space of the mould. The sandstone samples and CGFB were bonded into the sandstone-CGFB composite samples through the cement-fly ash slurry in CGFB. After 24 h, the composite samples were removed from the moulds and cured for 28 d in a curing box with a temperature of 20 ± 2 °C and a humidity of 80%. After curing, the ends of the CGFB in the composite samples were trimmed using a stone-grinding machine after cutting to create a smooth surface, and their sides were mechanically polished with the fine emery paper to obtain a diameter of 50 mm. At this stage, the sandstone-CGFB composite samples were well prepared.

2.3 Testing system

The testing system for uniaxial compression tests on the composite samples consisted of a loading system, an AE monitoring system, and a digital video camera (DVC), as shown in Fig. 3. During each test, the data from the loading system, AE monitoring system, and DVC were recorded simultaneously.

An AG-X250 servo-controlled testing system that could execute the conventional compression, tension, and other mechanical tests, was selected as the loading system (Chen *et al.* 2016, Yin *et al.* 2020, Chen *et al.* 2019b). The maximum testing load was 250 kN. A displacement loading mode was used at a loading rate of 0.0005 mm/s in these tests.

The AE event was selected to analyse the AE characteristics of composite samples during uniaxial loading, which was monitored by a MISTRAS AE instrument (Physical Acoustics Corporation, Princeton Jct, NJ, USA). The AE parameters are shown in Table 3. The pencil-lead fracture method proposed by ASTM (American Society for Testing and Materials) was employed to calibrate the AE system. When the AE amplitude signal was larger than 90 dB, these tests would be conducted. A SONY portable digital camera was used to record the failure characteristics of the sandstone-CGFB composite samples under uniaxial loading.

The sandstone-CGFB composite sample was an integrated body. During uniaxial loading, the sandstone and CGFB in the composite sample produced damage or fracture together. The resulting energy is released and transmitted via the material media and reflected by the receiving AE signals (Feng *et al.* 2019). While, in Table 2, the UCS of pure sandstone sample (40.178 MPa) was about 11.356 times that of pure CGFB sample (3.538 MPa). Therefore, the damage or fracture mainly occurred within the CGFB in the composite sample or along the interface between the sandstone and CGFB. In order to well observe the failure characteristics of sandstone-CGFB composite samples under uniaxial loading, one AE sensor was installed on the surface of the sandstone with the adhesive tape, and vaseline was applied on the contact area between the sensor and sandstone to warrant coupling conditions. The sandstone with a far higher strength than that of CGFB acted as a wave guide rod to transfer the AE signals to the AE sensor. Meanwhile, in the investigations on the AE characteristics of rock-coal composite samples under uniaxial loading, the AE signals collected from the AE sensor arranged on the surface of rock with a high strength were similar to that arranged on the surface of coal with a

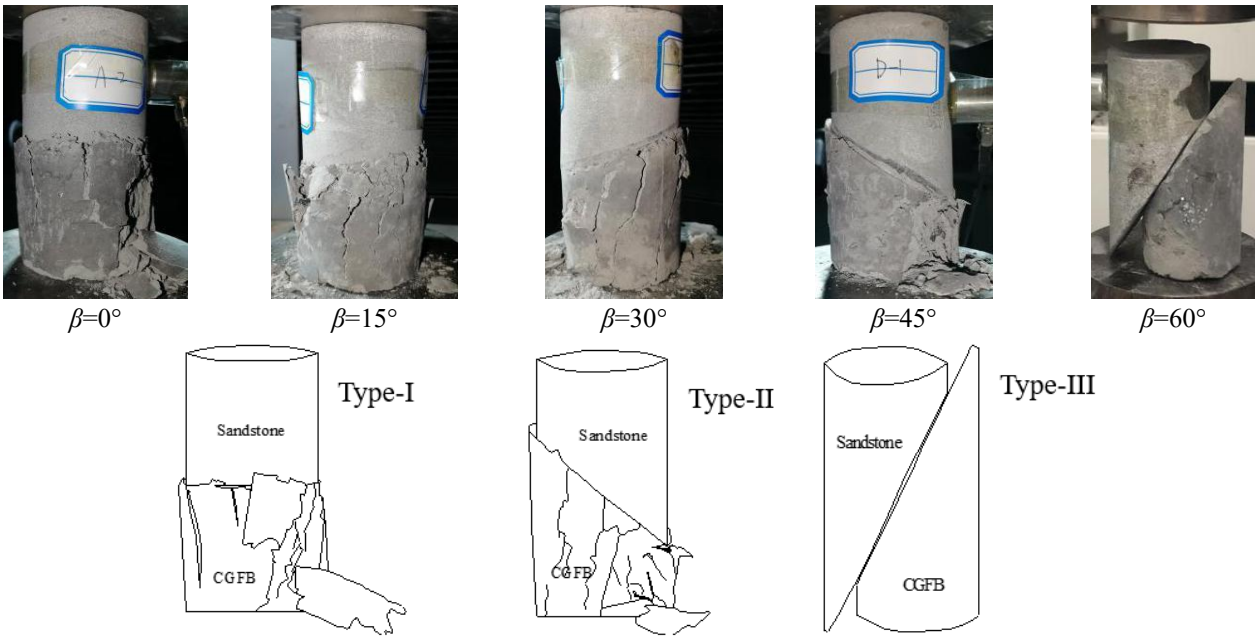

Fig. 4 Macro-failure patterns of the sandstone-CGFB composite samples

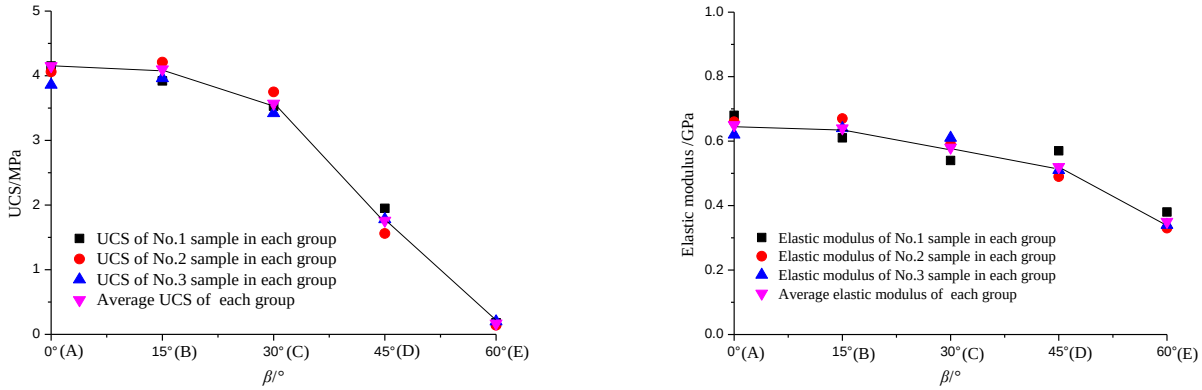

(a) UCS variation (b) Elastic modulus variation

Fig. 5 Variations in UCS and elastic modulus with β

low strength (Yin *et al.* 2018), and they well reflected the AE characteristics of composite samples. The AE sensor was generally installed on the surface of the rock in the rock-coal composite sample (Ren *et al.* 2010, Huang and Liu 2013).

3. Results

3.1 Failure characteristics of composite samples

Typical images of macro-failure exhibited on the sandstone-CGFB composite samples are shown in Fig. 4.

The interface angle affects the failure patterns of the composite samples. When β are 0°, 15°, and 30°, the failures of the composite samples mainly occur within the CGFB, and no obvious failure is observed in the sandstone. Obvious tensile cracks are identified in the CGFB, confirming a splitting failure, and varying degrees of local surface spalling failure zones are also observed on the CGFB. Therefore, the CGFB of the composite samples with β of 0°, 15°, and 30° mainly sustains the splitting failure accompanied by local surface spalling failures (Type-I failure). When β is 45°, the composite samples exhibit the mixed failure, i.e., the slight sliding failure along with the interface and Type-I failure (Type-II failure). In the Type-II failure, the CGFB initially sustains the Type-I failure, and then slight sliding failure along with the interface occurs. The corresponding sandstone shows no evidence of fracturing or failure. When β is 60°, the composite samples occur the sliding failure along with the interface (Type-III failure). The sandstone and CGFB are intact without obvious fracturing or failure. With an increase of β, the macro-failure pattern of composite sample changes from Type-I to Type-II, and then to Type-III.

3.2 Strength characteristics of composite samples

Fig. 5 shows the variations in the UCS and elastic modulus (the slope of stress-strain curve at 40%-60% of peak stress) of the sandstone-CGFB composite samples with β.

In Fig.5, there are almost no differences in UCS and elastic modulus between Groups A (β of 0°) and B (β of 15°). The average UCS and elastic modulus of Group C (β of 30°) are slightly lower than Groups A and B, and they decrease by 13.98% and 10.77%, respectively, compared with Group A. However, the average values of UCS and elastic modulus for Groups D (β of 45°) and E (β of 60°) show a large decrease. Compared with Group A, the average UCS and elastic modulus of Group D are 57.59% and 20.00% lower, respectively, and the corresponding average UCS and elastic modulus of Group E are 95.90% and 46.15% lower, respectively. According to the above analysis, the UCS and elastic modulus decrease overall with an increase of β, which can illustrate that the bearing capacity and deformation capacities of the composite samples are weakened with β under uniaxial loading.

3.3 AE characteristics of composite samples

Fig. 6 shows the AE characteristics of the sandstone-CGFB composite samples with different interface angles.

The deformation and failure processes of A-2, B-1, C-2, and D-1 composite samples can be categorized into four stages: the initial compaction stage, the linear elastic stage, the plastic yield stage, and the post-peak failure stage. Their AE characteristics in different stages are similar to that of pure CGFB composite samples. The initial compaction stage corresponds to the closures of the voids and cracks in the sandstone and CGFB, and the compression of the interface between them. CGFB is a manually configured material with more voids and cracks than natural sandstone. Therefore, in the initial compaction stage, the AE event signals exhibit large fluctuations in peak values, which differ from those of pure coal or rock samples, but are consistent with those of pure CGFB samples (Feng *et al.* 2019). During the linear elastic stage, the micro-cracks in the composite samples stably propagate, and the corresponding AE event signals attenuate with relatively smaller fluctuations compared with the initial compaction stage. Due to the unstable propagation of micro-cracks in the composite samples during the plastic yield stage, the AE event signals are re-enhanced and further intensified, exhibiting high fluctuations with large peak values. During the post failure stage, the micro-cracks coalesce, and many macro-cracks form in the composite samples. The propagation and coalescence of the macro-cracks cause the splitting failure of CGFB, accompanied by local surface spalling failure. However, in Fig. 6(a)-6(d), the AE event signals during the post-peak failure stage are re-weakened and have few peak values. This phenomenon was also observed in the AE characteristics of pure CGFB samples, mainly because the AE radiation waves were seriously attenuated and even blocked due to the aggregation of a large number of macro-cracks before failure (Qi and Feng 2015). Meanwhile, in the later post-peak failure stage in the D-1 composite sample, peak values of the AE event signals fluctuate due to the small sliding failure along with the interface.

The deformation and failure process of the E-2 composite sample is different from that of other composite samples. Before the initial compaction stage is completed, it sustains the sliding failure. The occurrence of the sliding failure along with the interface is not sudden. The corresponding post-peak stress-time curve initially exhibits a slow decrease, and when the sliding failure along with the interface is complete, it exhibits a steep linear drop as shown in Fig. 6(e). Some significant peaks in the AE event signals are found at the later stage of the sliding failure.

4. Discussions

The interface between the sandstone and CGFB in the composite sample can be considered as a single structural plane, inclined at an angle of β to the horizontal direction, as shown in Fig. 7(a). σ_1 is the uniaxial stress, σ_3 is the confining pressure, and σ and τ are the normal and shear stresses of the interface, respectively. It is assumed that the strength characteristics of the interface satisfy the Coulomb criterion, therefore (Zhao *et al.* 2016, Liang *et al.* 2020, Mohammadi and Tavakoli 2015),

$$\tau = C_i + \sigma \tan \phi_i \tag{1}$$

where C_i and ϕ_i are the cohesive force and internal friction angle of the interface, respectively.

The relationship between the Mohr stress circle and strength envelope can be used to analyse the failure characteristics of coal or rock samples. The relationships between strength envelopes and Mohr stress circles of the interface, sandstone, and CGFB are shown in Fig. 7(b). C_s and C_c are the cohesive forces of sandstone and CGFB, respectively, and ϕ_s and ϕ_c represent their internal friction angles, respectively. Sandstone has significantly higher strength compared to CGFB, i.e., $\sigma_{s1}>\sigma_{c1}$. This means that the failure of CGFB precedes that of sandstone in the composite sample, and the failures of the composite sample occur within CGFB. Therefore, the range of angle β should be based on the Mohr stress circle of the CGFB. The macro-failure patterns of composite samples were mainly determined by β. The A and B points are the intersections of the strength envelope of interface and Mohr stress circle of the CGFB. The N point is the centre of the Mohr stress circle of the CGFB. The included angle between NC line segment and σ axis is 2β. $2\beta_1$ and $2\beta_2$ are the included angles of the BN line segment, AN line segment, and σ axis (Zhao *et al.* 2016), respectively, as shown in Fig. 7 (b). Generally, when the value of 2β falls between $2\beta_1$ and $2\beta_2$, the composite sample failures tend to be the sliding failures along with the interface, otherwise composite sample failures occur within the CGFB

In this investigation, σ_3 is 0 MPa. In Fig. 7(b), as β increases from 0°, the stress point C falls between points A and B, 2β falls between $2\beta_1$ and $2\beta_2$, and the failure patterns of the composite samples change from failure within the CGFB to the sliding failure along with the interface. Evidently, the fracture plane approaches the interface until sliding failure induced by the compressive-shear stress and interfacial effect occurs along with the interface, i.e., with the continuous increase of β, this sliding phenomenon becomes increasingly apparent. In Fig. 4, following an increase in β from 0° to 60°, the failure patterns of the composite samples change from Type-I (splitting failure

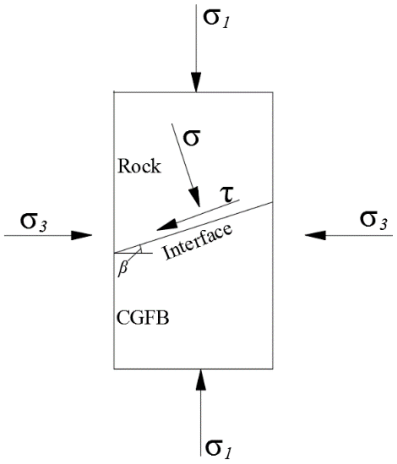

(a) Mechanical model for the composite sample

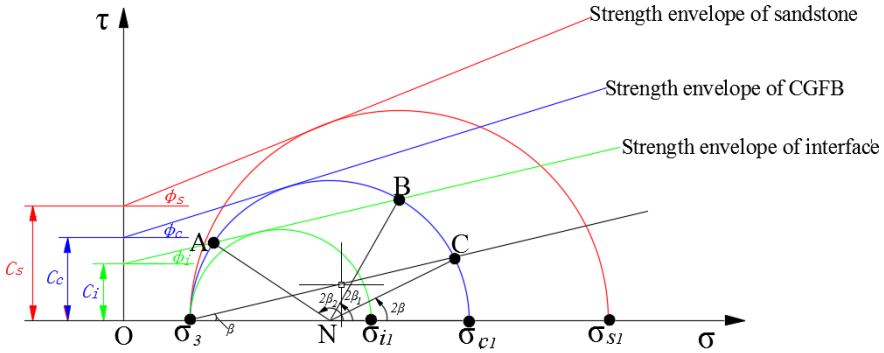

(b) Relationships between strength envelopes and Mohr stress circles of the interface, sandstone, and CGFB.

Fig. 7 Mechanical analysis of failures at the interface in a composite sample

accompanied by local spalling failure in CGFB) to Type-II (mixed failure along with sliding failure along with the interface and Type-I failure), and then to Type-III (sliding failure along with the interface), which are consistent with the results of the theoretical analysis.

The strength characteristics of the composite samples are related to their failure patterns. The failure pattern of Group E is Type-III, which shows that the strength of the interface between sandstone and CGFB mainly determines the overall strengths of the composite samples. Therefore, the corresponding strengths of Group E are the lowest in the five groups. The failure patterns of the composite samples at β of 0°, 15° and 30° are Type-I, i.e., the strengths of the composite samples depend on the strength of the CGFB. Therefore, the strength levels of Groups A, B, and C are relatively high. Although the sliding failure along with the interface does not occur in these composite samples, this tendency strongly increases when β ranges from 0° to 30°, which reduces the strength levels of the composite samples (Zhao *et al.* 2016; Pan *et al.* 2020). In particular, the strength level of Group C decreases compared with Groups A and B. The failure pattern of Group D is Type-II, i.e., the strength of the interface and CGFB determine the overall strength of the composite samples together. Therefore, the strength of Group D is higher than that of Group E, but lower than that of Groups A, B and C. The UCS of the composite sample with Type-I failure is the largest, and the UCS corresponding to Type-III failure is the lowest. With an increase of β, the UCS of the composite sample generally decreases.

5. Conclusions

This study aims to investigate the effects of interface angle on the strength, AE, and failure characteristics of sandstone-CGFB composite samples under uniaxial loading. The main conclusions are summarized as follows:

• The Three macro-failure patterns were exhibited by the composite samples: the splitting failure accompanied by the local spalling failure in CGFB (Type-I failure), the mixed failure with sliding failure along with the interface and Type-I (Type-II failure), and sliding failure along with the interface (Type-III failure). Following an increase in β from 0° to 60°, the macro-failure patterns changed from the Type-I to Type-II, and then to Type-III.

• With an increase in β from 0° to 60°, the UCS and elastic modulus of the composite sample decreased overall. The UCS of the composite sample with Type-I failure was the largest, and the UCS corresponding to the Type-III failure was the lowest. There were almost no differences in UCS and elastic modulus between Groups A (β of 0°) and B (β of 15°). The average UCS and elastic modulus of Group C (β of 30°) were slightly lower than Groups A and B, and they decreased by 13.98% and 10.77%, respectively, compared with Group A. Compared with Group A, the

average UCS and elastic modulus of Group D (β of 45°) decreased by 57.59% and 20.00%, respectively; and the corresponding UCS and elastic modulus of Group E (β of 60°) decreased by 95.90% and 46.15%, respectively.

• The deformation and failure processes of the composite samples can be categorized into the initial compaction stage, the linear elastic stage, the plastic yield stage, and the post-peak failure stage. Due to the small sliding failure along with the interface in the composite samples with a β of 45°, there were fluctuations in AE event signals with peak values in the later post-peak failure stage. The composite sample with a β of 60° sustained the sliding failure along with the interface before the completion of the initial compaction stage, which was not a sudden movement. The corresponding post-peak stress-time curve initially exhibited a slow decrease, and then sustained a steep linear drop with some significant peaks in AE event signals.

According to the test results, in the paste backfill mining, the bearing capacity and stability of the composite structure consisting of the immediate roof and CGFB body decrease with the interface angle between them measured horizontally. The sliding failure along with the interface occurs at a high interface angle. Under this conditions, the bolt support, anchor cable support and other methods should be adopted to enhance the integrity and stability of the composite structure. The bolts and anchor cables should be arranged through CGFB body at a certain angle to enter the interior of the immediate roof.

Acknowledgments

This work was supported by the National Key R&D Programme [grant number 2018YFC0604704], National Natural Science Foundation of China [grant numbers. 51904167, 52074169, 52004146; 51904149], Taishan Scholars Project, Taishan Scholar Talent Team Support Plan for Advantaged & Unique Discipline Areas, SDUST Research Fund, Open Research Fund of Key Laboratory of Safety and High-efficiency Coal Mining [grant number JYBSYS2019201], and Natural Science Foundation of Shandong Province [grant number 2019BEE013].

References

Ammirati, L., Mondillo, N., Rodas, R.A., Sellers, C. and Martire, D. (2020), "Monitoring land surface deformation associated with gold artisanal mining in the Zaruma City (Ecuador)", *Remote Sens*., **12**(13), 2135. https://doi.org/10.3390/rs12132135.

Bull, A.J. and Fall, M. (2020), "Curing temperature dependency of the release of arsenic from cemented paste backfill made with Portland cement", *J. Environ. Manage*., **269**, 110772. https://doi.org/10.1016/j.jenvman.2020.110772.

Cao, S., Yilmaz, E. and Song, W.D. (2019), "Fiber type effect on strength, toughness and microstructure of early age cemented tailings backfill", *Constr. Build. Mater*., **223**, 44-54. https://doi.org/10.1016/j.conbuildmat.2019.06.221.

Chang, X., Lu, J.Y., Wang, S.Y. and Wang, S.R. (2018), "Mechanical performances of rock-concrete bi-material disks under diametrical compression", *Int. J. Rock Mech. Min. Sci*., **104**, 71-77. https://doi.org/10.1016/j.ijrmms.2018.02.008.

Chen, S.J., Liu, X.Y., Han, Y., Guo, Y.H. and Ren, K.Q. (2016), "Experimental study of creep hardening characteristic and mechanism of filling paste", *Chin. J. Rock Mech. Eng*., **35**(3), 570-578 (In Chinese). https://doi.org/10.13722/j.cnki.jrme.2015.1228.

Chen, S.J., Yin, D.W., Jiang, N., Wang, F. and Guo, W.J. (2019a), "Simulation study on effects of loading rate on uniaxial compression failure of composite rock-coal layer", *Geomech. Eng*., **17**(4), 333-342. https://doi.org/10.12989/gae.2019.17.4.333.

Chen, S.J., Yin, D.W., Jiang, N., Wang, F. and Zhao, Z.H. (2019b), "Mechanical properties of oil shale-coal composite samples", *Int. J. Rock Mech. Min. Sci*., **123**, 104120. https://doi.org/ 10.1016/j.ijrmms.2019.104120.

Cui, B.Q., Liu, Y., Guo, H., Liu, Z.X. and Li, Y. (2018), "Experimental study on the durability of fly ash-based filling paste in environments with different concentrations of sulfates", *Adv. Mater. Sci. Eng*., 4315345. https://doi.org/10.1155/2018/4315345.

Du, X.J., Feng, G.R., Zhang, Y.J., Wang, Z.H., Guo, Y.X. and Qi, T.Y. (2019), "Bearing mechanism and stability monitoring of cemented gangue-fly ash backfill column with stirrups in partial backfill engineering", *Eng. Struct*., **188**, 603-612. https://doi.org/10.1016/j.engstruct.2019.03.061.

Ercikdi, B., Kesimal, A., Cihangir, F., Deveci, H. and Alp, I. (2009), "Cemented paste backfill of sulphide-rich tailings: Importance of binder type and dosage", *Cement Concrete Compos*., **31**(4), 268-274. https://doi.org/10.1016/j.cemconcomp.2009.01.008.

Feng, G.R., Du, X.J. and Zhang, Y.J. (2019), "Optical-acoustic-stress' responses in failure progress of cemented gangue-fly ash backfill material under uniaxial compression", *Nondestruct. Test Eval*., **34**(2), 135-146. https://doi.org/10.1080/10589759.2019.1576175.

Fishman, Y.A. (2008), "Features of shear failure of brittle materials and concrete structures on rock foundations", *Int. J. Rock Mech. Min. Sci*., **45**(6), 976-992. https://doi.org/10.1016/j.ijrmms.2007.09.011.

Fishman, Y.A. (2009), "Stability of concrete retaining structures and their interface with rock foundations", *Int. J. Rock Mech. Min. Sci*., **46**(6), 957-966. https://doi.org/10.1016/j.ijrmms.2009.05.006.

Huang, B.X. and Liu, J.W. (2013), "The effect of loading rate on the behavior of samples composed of coal and rock", *Int. J. Rock Mech. Min. Sci*., **61**, 23-30. https://doi.org/10.1016/j.ijrmms.2013.02.002.

Kaliyavaradhan, S.K., Ling, T.C., Guo, M.Z. and Mo, K.H. (2019), "Waste resources recycling in controlled low-strength material (CLSM): A critical review on plastic properties", *J. Environ. Manage*., **241**, 383-396. https://doi.org/10.1016/j.jenvman.2019.03.017.

Liang, P., Gao, Y.T., Zhou, Y., Zhu C. and Sun, Y.H., (2020), "Solution for surrounding rock of strain-softening considering confining pressure-dependent Young's modulus and nonlinear dilatancy", *Geomech. Eng*., **22**(4), 277-290. https://doi.org/10.12989/gae.2020.22.4.277.

Liu, Y., Lu, Y., Wang, C.X., Cui, B.Q., Guo, H., Li, H. and Guo, Y.L, (2018), "Effect of sulfate mine water on the durability of filling paste", *Int. J. Green Energy*, **15**(13), 864-873. https://doi.org/10.1080/15435075.2018.1529582.

Mbonimpa, M., Kwizera, P. and Belem, T. (2019), "Mine backfilling in the permafrost, part II: Effect of declining curing temperature on the short-term unconfined compressive strength of cemented paste backfills", *Minerals,* **9**(3), 172. https://doi.org/ 10.3390/min9030172.

Mohammadi, M. and Tavakoli, H. (2015), "Comparing the generalized Hoek-Brown and Mohr-Coulomb failure criteria for stress analysis on the rocks failure plane", *Geomech. Eng.*, **9**(1)115-124. https://doi.org/10.12989/gae.2015.9.1.115.

Ozdogan, M.V. and Deliormanli, A.H. (2020), "Determination of possible failure surfaces in an open-pit slope caused by underground production", *B. Geofis. Teor. Appl.*, **61**(2), 199-218. https://doi.org/10.4430/bgta0305.

Pan, H.Y., Yin, D.W., Jiang, N. and Xia, Z.G. (2020), "Crack initiation behaviors of granite specimens containing crossing-double-flaws with different lengths under uniaxial loading", *Adv. Civ. Eng.*, 8871335. https://doi.org/10.1155/2020/8871335.

Park, J.H., Edraki, M., Mulligan, D. and Jang, H.S. (2014), "The application of coal combustion by-products in mine site rehabilitation", *J. Clean. Prod.*, **84**, 761-772. https://doi.org/10.1016/j.jclepro.2014.01.049.

Qi, T.Y., Feng, G.R., Zhang, Y.J., Guo, J. and Guo, Y.X. (2015), "Effects of fly ash content on properties of cement paste backfilling", *J. Residuals Sci. Technol.*, **12**(3), 133-141.

Ren, A., Feng, G.R., Guo, Y.X., Qi, T.Y., Guo, J., Zhang, M., Kang, L.X., Han, Y.L. and Zhang, P.L. (2014), "Influence on performance of coal mine filling paste with fly ash", *J. China Coal Soc.*, **39**(12), 2374-2380. https://doi.org/10.jccs.2013.1747.

Ren, F.Q., Zhu, C. and He, M.C. (2010), "Moment tensor analysis of acoustic emissions for cracking mechanisms during schist strain burst", *Rock Mech. Rock Eng.*, **53**(1), 153-170. https://doi.org/10.1007/s00603-019-01897-3.

Scigala, R. and Szafulera, K. (2020), "Linear discontinuous deformations created on the surface as an effect of underground mining and local geological conditions-case study", *B. Eng. Geol. Environ.*, **79**(4), 2059-2068. https://doi.org/10.1007/s10064-019-01681-1.

Sivakugan, N., Rankine, R.M., Rankine, K.J. and Rankine, K.S. (2006), "Geotechnical considerations in mine backfilling in Australia", *J. Clean. Prod.*, **14**(12-13), 1168-1175. https://doi.org/10.1016/j.jclepro.2004.06.007.

Strzalkowski, P. and Szafulera, K. (2020), "Occurrence of linear discontinuous deformations in Upper Silesia (Poland) in conditions of intensive mining extraction-case study", *Energies*, **13**(8), 1897. https://doi.org/10.3390/en13081897.

Sujatha, V. and Kishen, J.M.C. (2003), "Energy release rate due to friction at bimaterial interface in dams", *J. Eng. Mech.*, **129**(7), 793-800. https://doi.org/10.1061/(ASCE)0733-9399(2003)129:7(793).

Sun, Q., Cai, C., Zhang, S.K., Tian, S., Li, B., Xia, Y.J. and Sun, Q.W. (2019), "Study of localized deformation in geopolymer cemented coal gangue-fly ash backfill based on the digital speckle correlation method", *Constr. Build. Mater.*, **215**, 21-331. https://doi.org/10.1016/j.conbuildmat.2019.04.208.

Tan, Y.L., Ma, Q., Zhao, Z.H., Gu, Q.H., Fan, D.Y., Song, S.L. and Huang, D.M. (2019), "Cooperative bearing behaviors of roadside support and surrounding rocks along gob-side", *Geomech. Eng.*, **18**(4), 439-448. https://doi.org/10.12989/gae.2019.18.4.439.

Tichavsky, R., Jirankova, E. and Fabianova, A. (2020), "Dating of mining-induced subsidence based on a combination of dendrogeomorphic methods and in situ monitoring", *Eng. Geol.*, **272**, 105650. https://doi.org/10.1016/j.enggeo.2020.105650.

Wang, C.X., Shen, B.T., Chen, J.T., Tong, W.X., Jiang, Z., Liu, Y. and Li, Y.Y. (2020), "Compression characteristics of filling gangue and simulation of mining with gangue backfilling: An experimental investigation", *Geomech. Eng.*, **20**(6), 485-495. https://doi.org/10.12989/gae.2020.20.6.485.

Wang, Y.B, Yin, D.W., Chen, S.J. Zhang, L.B., Liu, D.Y. and Sun, Y.H. (2020), "Experimental study on properties of rock-cemented coal gangue-fly ash backfill bimaterials with different coal gangue particle sizes", *Adv. Civ. Eng.*, 8820330. https://doi.org/10.1155/2020/8820330.

Wang, Z.C., Wang, Z.H. and Zhao, W.T. (2018), "Microscopic pore and filling performance of coal gangue cementitious paste", *J. Wuhan Univ. Technol. Mater. Sci.*, **33**(2), 427-430. https://doi.org/10.1007/s11595-018-1840-9.

Wu, D., Hou, Y.B., Deng, T.F., Chen, Y.Z. and Zhao, X.L. (2017), "Thermal, hydraulic and mechanical performances of cemented coal gangue-fly ash backfill", *Int. J. Miner. Process.*, **162**, 12-18. https://doi.org/10.1016/j.minpro.2017.03.001.

Xu, J.L., Xuan, D.Y., Zhu, W.B., Wang, X.Z., Wang, B.L. and Teng, H. (2015), "Study and application of coal mining with partial backfilling", *J. China Coal Soc.*, **40**(6), 1303-1312 (In Chinese). https://doi.org/10.13225/j.cnki.jccs.2015.3055.

Yin, D.W., Chen, S.J., Ge, Y. and Liu, R. (2020), "Mechanical properties of rock-coal bi-material samples with different lithologies under uniaxial loading", *J. Mater. Res. Technol.*, 2021, **10**, 322-338. https://doi.org/10.1016/j.jmrt.2020.12.010.

Yin, D.W., Chen, S.J., Xing, W.B., Huang, D.M. and Liu, X.Q. (2018), "Experimental study on mechanical behavior of roof-coal pillar structure body under different loading rates", *J. China Coal Soc.*, **43**(5), 1249-1257 (In Chinese). https://doi.org/10.13225/j.cnki.jccs.2017.1091.

Zhang, Q.L. and Wang, X.M. (2007), "Performance of cemented coal gangue backfill", *J. Cent. South Univ. Technol.*, **14**(2), 216-219. https://doi.org/10.1007/s11771-007-0043-y.

Zhang, X.G., Lin, J., Liu, J.X., Li, F. and Pang, Z.Z. (2017), "Investigation of hydraulic-mechanical properties of paste backfill containing coal gangue-fly ash and its application in an underground coal mine", *Energies*, **10**(9), 1309. https://doi.org/ 10.3390/en10091309.

Zhao, T.B., Guo, W.Y., Liu, C.P. and Zhao, G.M. (2016), "Failure characteristics of combined coal-rock with different interfacial angles", *Geomech. Eng.*, **11**(3), 345-359. https://doi.org/10.12989/gae.2016.11.3.345.

Zhong, H., Ooi, E.T., Song, C.M., Ding, T., Lin, G. and Li, H.J. (2014), "Experimental and numerical study of the dependency of interface fracture in concrete-rock specimens on mode mixity", *Eng. Fract. Mech.*, **124**, 287-309. https://doi.org/10.1016/j.engfracmech.2014.04.030.

Zhu, W.B., Xu, J.M., Xu, J.L., Chen, D.Y. and Shi, J.X. (2017), "Pier-column backfill mining technology for controlling surface subsidence", *Int. J. Rock Mech. Min. Sci.,* **96**, 58-65. https://doi.org/10.1016/j.ijrmms.2017.04.014.

Zhu, X.J., Guo, G.L., Liu, H., Chen, T. and Yang, X.Y. (2019), "Experimental research on strata movement characteristics of backfill-strip mining using similar material modeling", *B. Eng. Geol. Environ.*, **78**(4), 2151-2167. https://doi.org/10.1007/s10064-018-1301-y.

CC